The Astrophysical Journal, 696:1823–1833, 2009 May 10 doi:10.1088/0004-637X/696/2/1823

MAGNETO-THERMOHALINE MIXING IN RED GIANTS

Pavel A. Denissenkov[1,3], Marc Pinsonneault[1], and Keith B. MacGregor[2]
[1] Department of Astronomy, The Ohio State University, 4055 McPherson Laboratory, 140 West 18th Avenue, Columbus, OH 43210, USA; dpa@astronomy.ohio-state.edu, pinsono@astronomy.ohio-state.edu
[2] High Altitude Observatory, National Center for Atmospheric Research, P.O. Box 3000, Boulder, CO 80307-3000, USA; kmac@hao.ucar.edu
Received 2008 June 26; accepted 2009 February 21; published 2009 April 27

ABSTRACT

We revise a magnetic buoyancy model that has recently been proposed as a mechanism for extra mixing in the radiative zones of low-mass red giants. The most important revision is our accounting of the heat exchange between rising magnetic flux rings and their surrounding medium. This increases the buoyant rising time by five orders of magnitude; therefore, the number of magnetic flux rings participating in the mixing has to be increased correspondingly. On the other hand, our revised model takes advantage of the fact that the mean molecular weight of the rings formed in the vicinity of the hydrogen burning shell has been reduced by ^{3}He burning. This increases their thermohaline buoyancy (hence, decreases the total ring number) considerably, making it equivalent to the pure magnetic buoyancy produced by a frozen-in toroidal field with $B_\varphi \approx 10$ MG. We emphasize that some toroidal field is still needed for the rings to remain cohesive while rising. Besides, this field prevents the horizontal turbulent diffusion from eroding the μ contrast between the rings and their surrounding medium. We propose that the necessary toroidal magnetic field is generated by differential rotation of the radiative zone that stretches a preexisting poloidal field around the rotation axis, and that magnetic flux rings are formed as a result of its buoyancy-related instability.

Key words: stars: abundances – stars: evolution – stars: interiors

Online-only material: color figure

1. INTRODUCTION

During their first ascent on the red giant branch (RGB), a majority of low-mass stars (those with $M \lesssim 2\ M_\odot$) experience extra mixing in their radiative zones separating the H burning shell from the bottom of convective envelope (Sweigart & Mengel 1979; Charbonnel & Do Nascimento 1998; Denissenkov & VandenBerg 2003). Despite 30 years of effort, however, the underlying physical mechanism is still not understood. Observationally, the RGB extra mixing manifests itself through changes of the surface abundances of Li, C, N, and of the isotopic ratio ^{12}C/^{13}C correlating with an increasing luminosity (Gratton et al. 2000; Smith & Martell 2003). These changes are produced by the joint operation of thermonuclear reactions that take place in the vicinity of the H shell and a nonconvective mixing process that transports reaction products through the radiative zone to the convective envelope. Observations support the idea that this mixing process starts (or, gets much more efficient) when an RGB star reaches a luminosity at which the differential luminosity function for a population of stars having the same age and chemical composition shows a prominent bump (a local pile-up of stars). The luminosity bump results from a temporary slowing down of the star's evolution caused by its structural readjustment. This happens when the H shell crosses and erases a discontinuity in the H-abundance profile left behind by the bottom of convective envelope at the end of the first dredge-up. During the first dredge-up, which occurs on the subgiant branch and the lower RGB, the convective envelope grows in mass, which causes its bottom to penetrate the layers whose chemical composition had been altered yet on the main sequence (MS). This produces changes of the surface abundances of Li, C, N, and of the ^{12}C/^{13}C ratio similar to but by far less substantial than those incurred from the subsequent operation of the RGB extra mixing.

Until recently, it has been thought that the only reason why the RGB extra mixing does not manifest itself below the bump luminosity is a strong gradient of the mean molecular weight μ caused by the onset of a deep convective envelope (e.g., Charbonnel et al. 1998). Any mixing mechanism has to overcome the stable thermal stratification of the radiative zone, and in the presence of a positive ∇_μ such mixing is correspondingly more difficult. In an RGB star above the bump luminosity, the H shell has already crossed the H-profile discontinuity; therefore, the radiative zone is now chemically uniform everywhere except in a very close neighborhood of the H shell. This circumstance was repeatedly emphasized in the past. In particular, it has been used to model the RGB extra mixing with rotation-driven meridional circulation and turbulent diffusion. It was not until recently that it has become clear that rotational mixing fails to explain the chemical element transport in the radiative zones of upper RGB stars (Chanamé et al. 2005; Palacios et al. 2006). In short, this failure is due to the following main causes: firstly, rotation period measurements for young cluster stars and helioseismic data indicate that MS stars with $M \lesssim 1\ M_\odot$ lose a great amount of their initial angular momentum via magnetized stellar winds and that they most likely become slow and nearly solid-body rotators before leaving the MS; secondly, the chemical element transport by meridional circulation is strongly hindered by rotation-induced horizontal turbulence in stellar radiative zones (Chaboyer & Zahn 1992); thirdly, the vertical turbulent diffusion powered by differential rotation in the radiative zones of RGB stars operates at a low level too because it also redistributes the angular momentum, thus reducing the degree of differential rotation in a self-regulating way.

A new class of RGB extra mixing models has emerged since Eggleton et al. (2006) noticed that a tiny μ-gradient

[3] On leave from Sobolev Astronomical Institute of St. Petersburg State University, Universitetsky Pr. 28, Petrodvorets, 198504 St. Petersburg, Russia.

inversion ($\nabla_\mu \approx -10^{-4}$) becomes visible at the outer tail of the H burning shell precisely at the moment when the H shell erases the H-profile discontinuity. This inversion is produced by the reaction ^{3}He(^{3}He, 2p)^{4}He that locally reduces the mean molecular weight by $\Delta\mu \approx \mu^2 \Delta X_3/6$, where X_3 is the ^{3}He mass fraction. The mechanism can be effective in the low-mass RGB stars because their MS progenitors synthesize large amounts of ^{3}He in their outer radiative cores through nonequilibrium pp burning. Even though this ^{3}He-rich material gets diluted in the convective envelope during the first dredge-up, the radiative zone of a low-mass RGB star above the bump luminosity can still have X_3 increased up to a value of 2×10^{-3} (the solar initial ^{3}He abundance is 3×10^{-5}). For this mass fraction, the ^{3}He burning leads to $\Delta\mu \approx -10^{-4}$, assuming that $\mu \approx 0.6$ and $\Delta X_3 \approx -X_3$. Below the bump luminosity, the μ-gradient inversion is overridden by the strong positive μ-gradient built up on the MS. It shows up and may come into play only when the ^{3}He burning shell, advancing in mass in front of the major H shell, finds itself in the chemically homogeneous part of the radiative zone. This happens at the bump luminosity. Eggleton et al. (2006) found that a rapid mixing process occurred in their 3D simulations above this point, although the underlying cause was not identified (see Denissenkov & Pinsonneault 2008b).

Inspired by this work, Charbonnel & Zahn (2007a) have proposed that the μ-gradient inversion maintained by the ^{3}He burning drives thermohaline convection in the radiative zones of low-mass RGB stars above the bump luminosity and that this is the long-sought physical mechanism for the RGB extra mixing. Thermohaline convection is a mixing process triggered by a double diffusive instability (e.g., Vauclair 2004). Consider a stratified ideal gas with a stable temperature gradient ($\nabla \equiv d\ln T/d\ln P < \nabla_{\rm ad}$, where "ad" stands for adiabatic changes) but with an unstable composition gradient ($\nabla_\mu < 0$). If we isolate a gas blob and shift it up in the vertical direction then its further motion will depend on how fast the blob exchanges heat and composition with its surrounding medium horizontally. Indeed, the relative difference in density between the surrounding medium and the blob is $\Delta\rho/\rho \approx \Delta\mu/\mu - \Delta T/T$, assuming that $\Delta P = 0$. For the blob to continue rising, we need $\Delta\rho > 0$. Our assumptions about the gradients mean that $\Delta\mu > 0$ and $\Delta T > 0$ in the absence of both heat and molecular diffusion. Because these differences grow when the blob rises, $\Delta\rho$ may stay positive or it may ultimately become negative depending on the ratio $r_\mu = |\nabla_\mu|/(\nabla_{\rm ad} - \nabla)$. In our particular case, $r_\mu \ll 1$. Therefore, our idealized impermeable and adiabatic blob will rise a short distance and then stop, when the accumulated difference in T compensates that in μ. In reality, the heat exchange, whose rate is specified by the radiative diffusivity K, constantly works to reduce the difference in T. On the other hand, molecular diffusion $\nu_{\rm mol}$ tries to smooth out the difference in μ. The double diffusive instability may therefore develop only if $K \gg \nu_{\rm mol}$. In this case, the blob's rising speed can be estimated as $v \sim l/\tau_{\rm th}$, where l is the mean path that the blob travels before it gets dissolved, while $\tau_{\rm th} \sim d^2/K$ is the characteristic thermal timescale for a spherical blob of the diameter d. An approximate expression for the thermohaline diffusion coefficient can be obtained as $D_{\rm thc} \sim lvr_\mu \sim Kr_\mu(l/d)^2$. Charbonnel & Zahn (2007a) and Denissenkov & Pinsonneault (2008b) have demonstrated that the observed RGB mixing patterns can be explained by stellar evolutionary models with the ^{3}He-driven thermohaline convection only if $l/d \gtrsim 10$–30. A similarly large parameter ratio for thermohaline convection in stellar radiative zones was postulated by Ulrich (1972), as opposed to a ratio $l/d \sim 1$ advocated by Kippenhahn et al. (1980). Besides, the double-diffusive instability has been shown to result in formation of elongated (large l to d ratios) structures known as "salt fingers" in laboratory experiments with the saltier and warmer water overlying the fresher and colder water (Stern 1960).

However, there appears to exist observational and theoretical arguments challenging this model. First of all, a large number of old metal-poor MS stars with $M \lesssim 0.9\ M_\odot$, both in globular clusters and in the halo field, which had accreted He- and C-rich high-μ material from their evolved cluster or binary companions do not seem to have been thoroughly mixed by thermohaline convection (Newsham & Terndrup 2007; Denissenkov & Pinsonneault 2008a; Aoki et al. 2008), as it would be expected even if the less efficient prescription by Kippenhahn et al. (1980) were used for $D_{\rm thc}$. Second, thermohaline convection is expected to be suppressed by the rotation-induced horizontal turbulence that works together with the molecular diffusion to reduce the μ contrast between the rising gas blob and its surroundings (Denissenkov & Pinsonneault 2008b). Third, strong differential rotation is predicted to hinder thermohaline convection as well, because the "salt fingers" may be tilted by the rotational shear so rapidly that they will get damped before they produce significant mixing (Canuto 1999, and references therein). We anticipate that a similar effect is also produced by the Coriolis force in a uniformly rotating radiative zone. Contrary to these expectations, a much larger fraction of Li-rich objects has been found among rapidly rotating ($v \sin i \geqslant 8$ km s^{-1}) K giants than among their more common slowly rotating ($v \sin i \lesssim 1$ km s^{-1}) counterparts (Drake et al. 2002). The Li-rich K giants are low-mass stars located above the bump luminosity (Charbonnel & Balachandran 2000) in which large amounts of Li are thought to be synthesized via the ^{7}Be-transport mechanism (Cameron & Fowler 1971). To be efficient, this mechanism needs a 10 to 100 times faster mixing than that required to reproduce the abundance patterns in the majority of upper RGB stars (Denissenkov & Herwig 2004). It is not clear how thermohaline convection can explain the phenomenon of Li-rich K giants given that its efficiency should be lower in the more rapidly rotating stars. These arguments have motivated our search for an alternative RGB mixing mechanism.

In this paper, we use a simple model of toroidal magnetic field generation in a differentially rotating radiative zone of a bump luminosity RGB star to obtain order-of-magnitude estimates demonstrating that the buoyant rise of magnetic flux rings being formed close to the local minimum in μ may be a good alternative to the ^{3}He-driven thermohaline convection. A similar model has recently been proposed by Busso et al. (2007) (hereafter, referred to as BWNC). However, they assumed that a rising ring always stays in thermal equilibrium with its surrounding medium, and we argue that this leads to a substantial overestimate of the ring's radial velocity. We account for the impact of μ gradients and discuss the origin of the magnetic rings. We show that, as a mechanism for the RGB extra mixing, magnetic buoyancy has some advantages over thermohaline convection and, therefore, it is worth further investigating by means of multidimensional MHD simulations.

2. THE RGB STELLAR MODEL

Our background RGB stellar model, in the radiative zone of which the formation and buoyant rise of magnetic flux rings are studied, represents a typical metal-poor upper RGB star. It has the initial mass $M = 0.8\ M_\odot$, helium and heavy-element

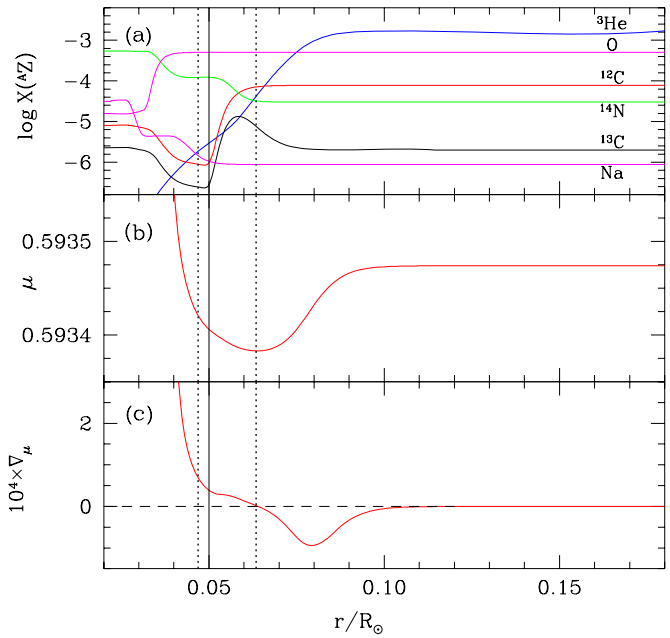

Figure 1. (a) Element mass fractions, (b) the mean molecular weight, and (c) its logarithmic (with respect to the pressure) gradient as functions of the radius in the vicinity of the H burning shell in our bump luminosity RGB model. The vertical solid line shows the observationally constrained depth of the RGB extra mixing $r_{\rm mix} = 0.05\ R_\odot$, the right dotted line—the radius $r_{\rm min}$ of the minimum μ, while the left dotted line is placed at $r = r_{\rm min} - H_P$.

(A color version of this figure is available in the online journal.)

mass fractions $Y = 0.24$ and $Z = 0.0005$, and the luminosity $\log L/L_\odot = 2.085$ corresponding to the age of 13.65 Gyrs. The RGB extra mixing is free to work in this star because the H burning shell has already erased the H-profile discontinuity in it. The model has been computed using the stellar evolution code described by Denissenkov et al. (2006). Its chemical element mass fraction, μ, and ∇_μ profiles immediately above the H shell are plotted in Figure 1.

For extra mixing to dredge up material deficient in C but not enriched in Na, as required by the observed abundance patterns in the metal-poor field RGB stars (Gratton et al. 2000), it has to reach a depth between 0.045 $R_\odot$ and 0.055 $R_\odot$ (Figure 1(a)). We will assume the mixing depth $r_{\rm mix} = 0.05\ R_\odot$ (shown by the vertical solid line in Figure 1). In previous works (e.g., Denissenkov & Weiss 1996; Denissenkov & VandenBerg 2003), the mixing depth was specified using either the relative mass coordinate $\delta M_{\rm mix} = (M_{\rm mix} - M_{\rm c})/(M_{\rm bce} - M_{\rm c})$ or the logarithmic temperature difference $\Delta \log T = \log T(r_{\rm c}) - \log T(r_{\rm mix})$, where the subscripts "c" and "bce" refer to the He core boundary and to the bottom of convective envelope, respectively. However, we have noticed that, when plotted as functions of r, the abundance profiles remain nearly stationary in spite of the slow mass inflow from the radiative zone that feeds the H burning shell. Therefore, we have decided to simply use the radius for the RGB mixing depth specification. The value of $r_{\rm mix} = 0.05\ R_\odot$ corresponds to $\delta M_{\rm mix} = 0.135$ and $\Delta \log T = 0.245$.

For subsequent estimates of various quantities characterizing the efficiencies of magnetic flux ring formation and buoyant rise in the radiative zone of our RGB model, we need to know some of its structure parameters at $r = r_{\rm mix}$. These are summarized in Table 1 along with the parameter values at $r = r_{\rm bce}$. We have also listed the values used by BWNC. Note that they have considered a half-solar metallicity bump luminosity model with the initial mass of 1.5 $M_\odot$.

3. ROTATION IN THE RADIATIVE ZONE

In our magnetic buoyancy model, it is assumed that a toroidal magnetic field in the radiative zone of an RGB star is generated by its differential rotation that stretches a preexisting poloidal field around the rotation axis. To elaborate on the model, we therefore need an estimate of the degree of differential rotation in the radiative zone. For this, we use the rotation profile M2 presented by Palacios et al. (2006) in their Figure 2 (the dotted curve in upper panel C). It shows the angular velocity Ω as a function of $\delta M = (M_r - M_{\rm c})/(M_{\rm bce} - M_{\rm c})$ in the radiative zone of a bump luminosity model with initial values of M, Y, and Z almost identical to ours. The model's rotational evolution was computed using the stellar evolution code STAREVOL designed for 1D simulations of the angular momentum and chemical element transport in stellar radiative zones (Siess et al. 2000; Palacios et al. 2003). The code takes proper account of the rotation-induced meridional circulation, horizontal and vertical turbulent diffusion, as well as atomic diffusion and mass loss. The initial zero-age MS model for the M2 run has been assumed to be a slow solid-body rotator with the surface

Table 1
RGB Model Structure Parameters

Parameter	Units	Our Model		BWNC Model	
		$r_{\rm mix} = 0.0500\ R_\odot$	$r_{\rm bce} = 0.996\ R_\odot$	$r_{\rm mix} = 0.0495\ R_\odot$	$r_{\rm bce} = 0.912\ R_\odot$
M_r	$M_\odot$	0.309	0.331	0.252	0.256
H_P	r	0.257	0.449	0.371	0.622
μ	AMU	0.593406	0.593474		
T	K	2.16×10^7	2.02×10^6	2.51×10^7	2.26×10^6
ρ	g cm^{-3}	14.8	1.03×10^{-2}	5.19	2.55×10^{-3}
P	dyn cm^{-2}	4.49×10^{16}	2.93×10^{12}	1.87×10^{16}	8.49×10^{11}
K	cm^2 s^{-1}	9.35×10^7	8.15×10^{10}		
N_T^2	s^{-2}	5.40×10^{-4}	1.13×10^{-9}		
N_μ^2	s^{-2}	1.48×10^{-7}	0.00		
$\nu_{\rm mol}$	cm^2 s^{-1}	1.80×10^2	6.76×10^2		
$\nu_{\rm rad}$	cm^2 s^{-1}	1.74×10^2	1.43×10^4		
η	cm^2 s^{-1}	19.3	6.90×10^2		
κ	cm^2 g^{-1}	0.382	0.728		
$\lvert\dot{r}\rvert$	cm s^{-1}	3.91×10^{-5}	8.50×10^{-5}		
Ω	rad s^{-1}	10^{-3}	10^{-6}		

rotational velocity of 5 km s^{-1}. This choice is a reasonable replacement for detailed computations of the pre-MS and early MS evolution during which a low-mass star experiences a strong magnetic breaking of its much faster initial surface rotation and a core-envelope rotational coupling leading to its nearly uniform internal rotation on a much shorter timescale than its MS lifetime.

Another important assumption made by Palacios et al. (2006) is uniform specific angular momentum distribution in the RGB convective envelope. This is required to explain the origin of rapidly rotating red horizontal branch stars (Sills & Pinsonneault 2000). This empirical demand for a strong differential rotation in the convective envelopes of low-mass RGB stars is supported by recent 3D hydrodynamic simulations of the interaction of turbulent convection and rotation performed by Palacios & Brun (2006).

The M2 bump luminosity model has $\Omega(r_{\rm bce}) \approx 10^{-6}$ rad s^{-1}, and $\Omega(r_{\rm mix}) \approx 10^{-3}$ rad s^{-1}. We will use these values in our following discussion. So, in the absence of transport processes other than those considered by Palacios et al. (2006), the angular velocity in the radiative zone of our RGB stellar model could vary with the radius approximately as $\Omega(r) = \Omega(r_{\rm mix})(r_{\rm mix}/r)^2$. This steep rotation profile results from the conservation of angular momentum in the mass inflow and modest angular momentum redistribution by meridional circulation and vertical turbulent diffusion.

4. SUPPRESSION OF THERMOHALINE CONVECTION BY HORIZONTAL TURBULENCE

Denissenkov & Pinsonneault (2008b) have derived a general criterion for convective instability in the presence of a negative ∇_μ and strong horizontal turbulence, the latter being characterized by a diffusion coefficient $D_{\rm h} \gg \nu_{\rm mol}$. They have allowed for a possibility that a convective element of the diameter d can travel a distance $l > d$. One of the consequences of this criterion is that thermohaline convection may be suppressed by the horizontal turbulent diffusion unless

$$\frac{|\nabla_\mu|}{\nabla_{\rm rad} - \nabla_{\rm ad}} > \frac{1}{3}\frac{D_{\rm h}}{K + D_{\rm h}}, \quad (1)$$

where $\nabla_{\rm rad}$ is the radiative temperature gradient (compare this inequality with condition 5 from Vauclair 2004). Note that a similar result can be obtained from the dispersion relation (10) derived and analyzed by Ulrich (1972). One should only take into account that, in the presence of the strong horizontal turbulence, Ulrich's molecular diffusion coefficient $\mathbf{D}$ has to be replaced with $D_{\rm h}$. Then, for the thermally limited modes, one readily finds

$$D_{\rm thc} \approx D_{\rm Ulrich} \times \left(1 - \frac{D_{\rm h}}{K}\frac{\nabla_{\rm rad} - \nabla_{\rm ad}}{|\nabla_\mu|}\right), \quad (2)$$

where $D_{\rm Ulrich}$ is Ulrich's original thermohaline diffusion coefficient. From the last expression it follows that thermohaline convection may operate ($D_{\rm thc} > 0$) only when $|\nabla_\mu|/(\nabla_{\rm ad} - \nabla_{\rm rad}) > D_{\rm h}/K$, which is close to the requirement (1), provided that $D_{\rm h} < K$. The difference in the right-hand-side ratios between the two conditions comes about from the fact that, unlike Denissenkov & Pinsonneault (2008b), Ulrich neglected the contribution of $\mathbf{D}$ to the heat diffusion. That was warranted for the nonrotating case considered by him, in which $D_{\rm h} = 0$, and therefore $\mathbf{D} = \nu_{\rm mol} \ll K$.

Palacios et al. (2006) have shown that $D_{\rm h}$ always stays comparable to K at $r \approx r_{\rm mix}$ in their M2 RGB model. Moreover, the ratio $D_{\rm h}/K$ turns out to be larger than $\sim 10^{-3}$ at all radii between $r_{\rm mix}$ and $r_{\rm bce}$, both in the bump luminosity model and in the more evolved model shown in their Figure 5 (panels C and D). Given that the ^{3}He burning can make the ratio $|\nabla_\mu|/(\nabla_{\rm rad} - \nabla_{\rm ad}) \sim 10^{-3}$ at most, while the RGB extra mixing will necessarily reduce it below this limit (by smoothing out the μ-gradient), the linear analysis predicts that thermohaline convection may be suppressed in these models, especially in the vicinity of $r_{\rm mix}$. It would be inconsistent to ignore this prediction because similar eroding effects of the horizontal turbulence on the model rotational and mixing properties have already been included in the simulations performed by Palacios et al. (2006). They are responsible for the significant reduction of the efficiency of mixing by meridional circulation (Chaboyer & Zahn 1992) and for the erasing of the latitudinal differential rotation, the latter effect allowing to consider Ω as a function of r alone (Zahn 1992). Besides, Zahn's concept of the rotation-induced anisotropic turbulence in stellar radiative zones, with horizontal components of the turbulent viscosity strongly dominating over those in the vertical direction, was repeatedly used in stellar evolution computations to facilitate the penetration of μ-gradient barriers by the vertical turbulent diffusion in both MS stars and upper RGB stars (Talon & Zahn 1997; Talon et al. 1997; Maeder 2003; Palacios et al. 2003, 2006).

5. GENERATION OF TOROIDAL MAGNETIC FIELD

Following Mestel & Weiss (1987), we assume that, like in the solar-type MS stars, the differential rotation in the radiative zone of the RGB star creates a toroidal magnetic field B_φ by shearing a preexisting constant poloidal field $\mathbf{B}_{\rm p} = \{B_r,\ B_\theta,\ 0\}$ (we use the spherical polar coordinates). As a result of its buoyancy-related undular instability (e.g., Acheson 1978; Spruit & van Ballegooijen 1982), the toroidal field is prompted to form magnetic flux rings that will rise toward the bottom of convective envelope, thus producing chemical mixing and also participating in angular momentum redistribution.

At the stellar equator ($\theta = 90^\circ$), the momentum and induction equations (Charbonneau & MacGregor 1993) can be reduced to

$$\frac{\partial \Omega}{\partial t} = \omega_{{\rm A},r}^2 \frac{\partial b}{\partial r}, \quad (3)$$

$$\frac{\partial b}{\partial t} = r^2 \frac{\partial \Omega}{\partial r}, \quad (4)$$

where $\omega_{{\rm A},r} = B_r/(\sqrt{4\pi\rho}\, r)$ is the local Alfvén frequency associated with the radial field component B_r, and $b = r B_\varphi / B_r$. In Equations (3) and (4), we have omitted the viscosity and magnetic diffusivity, for these will be shown to work on much longer timescales than the formation and buoyant rise of magnetic rings. For the sake of simplicity, we have additionally assumed that the poloidal field's configuration is such that $B_\theta = 0$ at the equator. Neglecting changes with the radius of the coefficients in Equations (3) and (4), we find that the variations of Ω and b can locally be described by the same Alfvén wave equation

$$\frac{\partial^2 f}{\partial r^2} - \frac{1}{\left(r^2 \omega_{{\rm A},r}^2\right)}\frac{\partial^2 f}{\partial t^2} = 0.$$

So, at a given radius, the initial (continuing while $t \ll \omega_{{\rm A},r}^{-1}$) decrease of Ω and increase of $|b|$ can be approximated as

$\Omega(t, r) \approx \Omega_{\max}(r)\cos(\omega_{A,r}\, t)$, and $b(t, r) \approx b_{\max}(r)\sin(\omega_{A,r}\, t)$. From Equations (3) and (4), we can also estimate the ratio of the wave amplitudes $\Omega_{\max}/b_{\max} \approx \omega_{A,r}/r$, hence $(B_\varphi)_{\max} \approx B_r(\Omega_{\max}/\omega_{A,r})$. This ensures that the sum of the rotational kinetic and toroidal field potential energy (per unit gram) is conserved,

$$\frac{1}{2}(r\Omega)^2 + \frac{B_\varphi^2}{8\pi\rho} = \frac{1}{2}(r\Omega_{\max})^2. \quad (5)$$

Substituting the values of $r = r_{\rm mix}$ and $\rho = \rho(r_{\rm mix})$ from our RGB model (Table 1) into the above relations, we find that

$$\omega_{A,r}^{-1} = 1.50 \times 10^3\, B_r^{-1}\ \ {\rm yr\ rad^{-1}}, \quad (6)$$

$$(B_\varphi)_{\max} = 4.75 \times 10^5\, (\Omega_{\max})_{-5}\, B_r, \quad (7)$$

where $(\Omega_{\max})_{-5} \equiv \Omega_{\max}/(10^{-5}\ {\rm rad\ s^{-1}})$. Equation (7) gives an order-of-magnitude estimate of the toroidal field maximum strength that may be generated by the differential rotation at $r = r_{\rm mix}$, while Equation (6) estimates its growth time. For example, we may expect (from Equation (4)) that, after a time $\Delta t \ll \omega_{A,r}^{-1}$, a toroidal field $B_\varphi \approx \Omega_{\max} B_r\, q\, \Delta t \approx (B_\varphi)_{\max}\, \omega_{A,r}\, q\, \Delta t = 3.16 \times 10^2 (\Omega_{\max})_{-5} B_r\, q\, \Delta t$ will be created, where $q = (\partial \ln\Omega/\partial \ln r) < 0$ is the initial rotational shear, and Δt is expressed in years. Assuming that $\Omega_{\max} = \Omega(r_{\rm mix}) = 10^{-3}$ rad s^{-1} (Table 1) at the moment when the differential rotation begins to stretch the poloidal field, we obtain the estimate

$$B_\varphi(\Delta t,\ r_{\rm mix}) \approx 3.16 \times 10^4 B_r\, q\, \Delta t, \quad (8)$$

where $\Delta t \ll 1.50 \times 10^3\, B_r^{-1}$ yrs. The relative decrease of Ω for the same period of time is $|\Delta\Omega/\Omega_{\max}| \approx 4.42 \times 10^{-7} B_r^2 q^2 (\Delta t)^2 \ll 1$. In the general case of $B_\theta \neq 0$ and $\Omega = \Omega(r, \theta)$ we would have $B_\varphi \approx r\sin\theta\, (\nabla\Omega, \mathbf{B}_{\rm p})\, \Delta t$ for $\Delta t \ll \omega_{A,r}^{-1}$ (Spruit 1999), i.e., both poloidal field components would be involved into the winding up of toroidal field.

If the uniform rotation of the solar radiative core and the core-envelope rotational coupling in the low-mass MS stars are both produced by the back reaction of the azimuthal component of the Lorentz force emerging in the process of generation of toroidal magnetic fields by the shearing of preexisting poloidal fields, as proposed by Charbonneau & MacGregor (1993), then the MS progenitors of low-mass RGB stars are required to possess poloidal magnetic fields with strengths of the order of 0.01 G to 10 G in their radiative interiors. The low magnetic diffusivity $\eta \sim 10^2$ sm^2 s^{-1} in the low-mass MS stars excludes the ohmic dissipation of these fields. Therefore, the post-MS contraction of the H-exhausted core from its MS radius of $\sim 0.2\ R_\odot$ down to its RGB radius $r_c \approx 0.02\ R_\odot$ and magnetic flux conservation might lead to the amplification of B_r up to the values 17 G to 1 kG. From the same considerations, it also follows that B_r in the radiative zone of the RGB star may decrease with the radius as $B_r \approx B_r(r_{\rm mix})(r_{\rm mix}/r)^2$. It is true that the mass inflow in the radiative zone may sweep the frozen-in poloidal field toward the H burning shell on a long timescale of the order of $\Delta r/|\dot r| = (r_{\rm bce} - r_{\rm mix})/|\dot r| \sim 3 \times 10^7$ yrs (Table 1). However, the poloidal field may be replenished by a dynamo operating at the bottom of convective envelope. It may then be entrained and redistributed all over the radiative zone by the mass inflow, which could also produce the dependence $B_r \propto r^{-2}$. These estimates will be used in our further analysis.

6. THE BUOYANT RISE OF MAGNETIC FLUX RINGS

6.1. General Results

Because we assume a differential rotation in the radiative zone, the inertial frame of reference has been chosen. The magnetic flux rings are assumed to be axisymmetric with respect to the rotation axis. In the spherical polar coordinates, their radial and latitudinal accelerations are

$$\frac{du_r}{dt} = \frac{u_\theta^2}{r} + \left(\frac{u_\varphi^2}{r} - \Omega^2 r\sin^2\theta\right) + \frac{\rho_{\rm e} - \rho}{\rho_{\rm e} + \rho}\left(\frac{GM_r}{r^2} - \Omega^2 r\sin^2\theta\right) - \frac{B_\varphi^2}{4\pi r(\rho_{\rm e} + \rho)} - \frac{C_{\rm D}}{\pi a}\frac{\rho_{\rm e}}{\rho_{\rm e} + \rho} u_r\sqrt{u_r^2 + u_\theta^2}, \quad (9)$$

$$\frac{du_\theta}{dt} = -\frac{u_r u_\theta}{r} + \left(\frac{u_\varphi^2}{r}\cot\theta - \Omega^2 r\sin\theta\cos\theta\right) - \frac{\rho_{\rm e} - \rho}{\rho_{\rm e} + \rho}\,\Omega^2 r\sin\theta\cos\theta - \frac{B_\varphi^2}{4\pi r(\rho_{\rm e} + \rho)}\cot\theta - \frac{C_{\rm D}}{\pi a}\frac{\rho_{\rm e}}{\rho_{\rm e} + \rho} u_\theta\sqrt{u_r^2 + u_\theta^2}. \quad (10)$$

These equations (Choudhuri & Gilman 1987; MacGregor & Cassinelli 2003; MacDonald & Mullan 2004) take into account the centrifugal reduction of the local gravitational acceleration, the buoyant force, the magnetic tension force, and the aerodynamic drag force (we employ the drag coefficient $C_{\rm D} = 1$). They are supplemented with the equation

$$\frac{d}{dt}(u_\varphi r\sin\theta) = 0 \quad (11)$$

describing the conservation of the azimuthal component of the specific angular momentum. The subscript "e" means that the respective quantity is referred to the external medium surrounding the rings, while all other quantities, except Ω, refer to ring properties.

At its starting position $(r_0,\ \theta_0)$, a ring is specified by its initial cross-section radius a_0, the strength of the frozen-in toroidal magnetic field $B_{\varphi,0}$, and internal thermodynamic properties P_0, T_0, ρ_0, and μ_0. The dynamic equilibrium between the ring and its surrounding medium requires that

$$P_{\rm e} = P + \frac{B_\varphi^2}{8\pi},\ \ {\rm or}\ \ \frac{\Delta P}{P_{\rm e}} \equiv \frac{(P_{\rm e} - P)}{P_{\rm e}} = \frac{1}{(1 + \beta)} \approx \frac{1}{\beta}, \quad (12)$$

where $\beta \equiv P/(B_\varphi^2/8\pi) \gg 1$ is the ratio of the thermodynamic to magnetic pressure in the ring. The conservation of mass and magnetic flux of the ring determine how its radius and toroidal field evolve during its motion

$$\left(\frac{a}{a_0}\right)^2 = \frac{\rho_0 r_0\sin\theta_0}{\rho r\sin\theta} = \frac{B_{\varphi,0}}{B_\varphi}, \quad (13)$$

where $r_0 \leqslant r \leqslant r_{\rm bce}$. For the equation of state, we use the ideal gas law. Finally, the entropy change in the ring is described by the simple equation

$$\frac{dS}{dt} = \frac{32(\gamma - 1)\sigma T_{\rm e}^4}{3\kappa_{\rm e}\rho_{\rm e} a^2 P}\,\delta T = 2\gamma K\,\frac{\delta T}{a^2} \quad (14)$$

derived by MacGregor & Cassinelli (2003). Here, $S = \ln[(P/P_0)(\rho_0/\rho)^\gamma]$, $\delta T = (T_{\rm e} - T)/T_{\rm e}$, and $\gamma = 5/3$.

Table 2
Magnetic Flux Ring Parameters

Parameter	Units	Our Model ($\Delta\mu = 5 \times 10^{-5}$)		BWNC Model ($\Delta\mu = 0$)	
		$B_r = 7.3$ G	$B_r = 73$ G	RGB-1	RGB-2
a_0	cm	1.3×10^7	9.7×10^6	6.5×10^6	1.5×10^7
a_0	H_P	1.5×10^{-2}	1.1×10^{-2}	5.1×10^{-3}	1.2×10^{-2}
t_b	yr	2.9×10^2	1.6×10^2	0.19	1.1
$\langle v_b \rangle$	cm s^{-1}	7.3	13	9.8×10^3	1.8×10^3
$(B_\varphi)_0$	kG	254	254	380	48
β_0		1.8×10^7	1.8×10^7	3.3×10^6	2.0×10^8
$(B_\varphi)_{bce}$	kG	3.5	3.5	3.5	0.44
N		1.3×10^2	1.3×10^2	1.0	1.0
$\dot{N} = N/t_b$	yr^{-1}	0.45	0.83	5.3	0.91

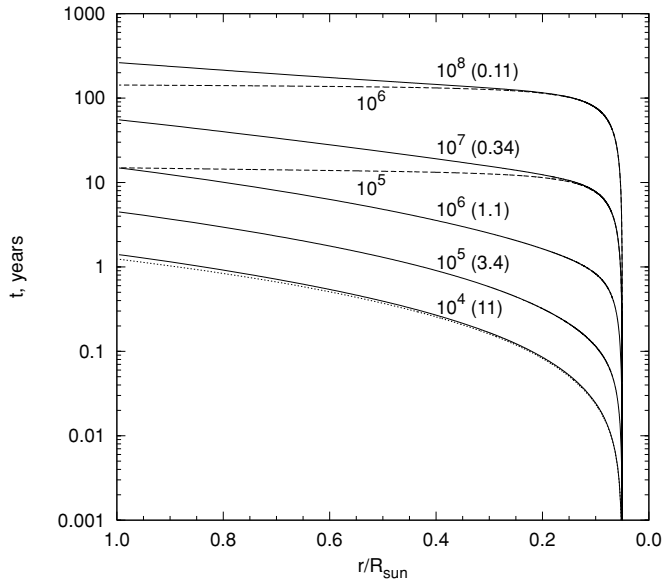

Figure 2. Motion of the equatorial magnetic flux rings with the cross-section radii $a_0 = 10^{-4}\,H_P$ (solid and dotted curves) and $a_0 = 10^{-3}\,H_P$ (dashed curves). The powers of ten show the specified values of β_0, while the numbers in parentheses give the corresponding strengths (in MG) of the frozen-in toroidal magnetic field. The dotted curve corresponds to the ring with $\beta_0 = 10^{10}$ ($B_\varphi \approx 11$ kG) whose mean molecular weight has been reduced by $\Delta\mu = 5 \times 10^{-5}$.

The initial conditions for the ring are specified by $r_0 = r_{mix} = 0.05\,R_\odot$, $0 < \theta_0 \leqslant 90^\circ$, $u_r = 0$, $u_\theta = 0$, $u_\varphi = r_0 \sin\theta_0\,\Omega(r_0, \theta_0)$, $\beta = \beta_0$, $a = a_0$, $S = 0$, $\delta P \equiv (P_e - P)/P_e = (1 + \beta_0)^{-1}$, $\delta\rho \equiv (\rho_e - \rho)/\rho_e = (1 + \beta_0)^{-1}$, and $\delta T = 0$. The ring's radius a will be measured in units of the local pressure scale height $H_P = P_e/g\rho_e$, where $g = GM_r/r^2$ is the gravitational acceleration. The implicit assumption of uniform pressure inside the ring requires that $a \ll H_P$ (the thin ring approximation). For brevity, we will denote $a \equiv (a/H_P)$ and, given the previous remark, will only consider cases with $a \ll 1$.

The above differential and algebraic equations have been solved numerically. The motion of the ring in the equatorial plane ($\theta_0 = 90^\circ$) is shown in Figure 2 for our assumed rotation law $\Omega(r, \theta) = \Omega(r_{mix})(r_{mix}/r)^2$, in which case $\theta(t) = \theta_0$. Solid curves correspond to the initial value of $a_0 = 10^{-4}$, while dashed curves have $a_0 = 10^{-3}$. The powers of ten near the curves give their specified values of β_0, the respective toroidal field strengths (in MG) being displayed in parentheses. Our computations have shown that for $\beta_0 \gtrsim 10^8$ (in other words, for $(B_\varphi)_0 \lesssim 0.1$ MG) and $a_0 \gtrsim 2 \times 10^{-4}$ the dependence of the total buoyant rising time on β_0 and a_0 can be approximated as

$$t_b \approx 1.4 \times 10^2 \left(\frac{\beta_0}{10^8}\right) \left(\frac{a_0}{10^{-4}}\right)^2 \text{ yr}. \quad (15)$$

This is transformed into the average buoyant velocity

$$\langle v_b \rangle = \frac{\Delta r}{t_b} = \frac{(r_{bce} - r_{mix})}{t_b} \approx 15 \left(\frac{10^8}{\beta_0}\right) \left(\frac{10^{-4}}{a_0}\right)^2 \text{ cm s}^{-1}, \quad (16)$$

which is nearly five orders of magnitude smaller than the appropriately scaled average velocity used by BWNC (for the scaling, we have used the data from the fifth column of Table 1 and the column RGB-1 of Table 2). We have tested that this big difference is entirely caused by the assumption of thermal equilibrium between the ring and its surroundings made in the cited paper.

The dashed and dot-dashed curves in Figure 3 show the dependences of t_b on a_0 for $\beta_0 = 10^8$ and $\beta_0 = 10^7$ obtained by solving Equations (9)–(11), while the dotted lines represent their approximations by (15). It is seen that the exact solutions strongly deviate from the approximate ones at $a_0 \lesssim 2 \times 10^{-4}$. This limit corresponds to a regime in which the aerodynamic drag force comes into play. Indeed, the last terms on the right-hand sides of Equations (9) and (10), which describe the drag force, are negative and inversely proportional to a. They lead to a slowing down of the ring's buoyant rise at small a, which is not reflected in Equation (15).

6.2. *Rings with μ Reduced by ^{3}He Burning*

Our numerical computations can optionally take into account the fact that the rings carrying the nuclear processed material are necessarily formed in the region of the local μ depression maintained by the ^{3}He burning (Figure 1(b)). They must therefore have a lower μ than the bulk of the radiative zone through which they move. As a result, their average buoyant velocity is found to weakly depend on the toroidal field strength. However, the frozen-in toroidal field is still needed for them to remain cohesive while rising.

The dotted curve in Figure 2 shows the path of a ring with $\Delta\mu = \mu_e - \mu = 5 \times 10^{-5}$, $a_0 = 10^{-4}$, and $\beta_0 = 10^{10}$ that corresponds to $(B_\varphi)_0 \approx 11$ kG. Its buoyant rising time is $t_b \approx 1.3$ yrs. Approximately, the same short time is obtained for a ring with $(B_\varphi)_0 \approx 1.1$ kG ($\beta_0 = 10^{12}$). If those two rings had $\mu = \mu_e$ then their rising times would be much longer and vastly different, namely, $t_b \approx 10^4$ yrs and $t_b \approx 10^6$ yrs, respectively (Equation (15)). This means that their buoyancy is

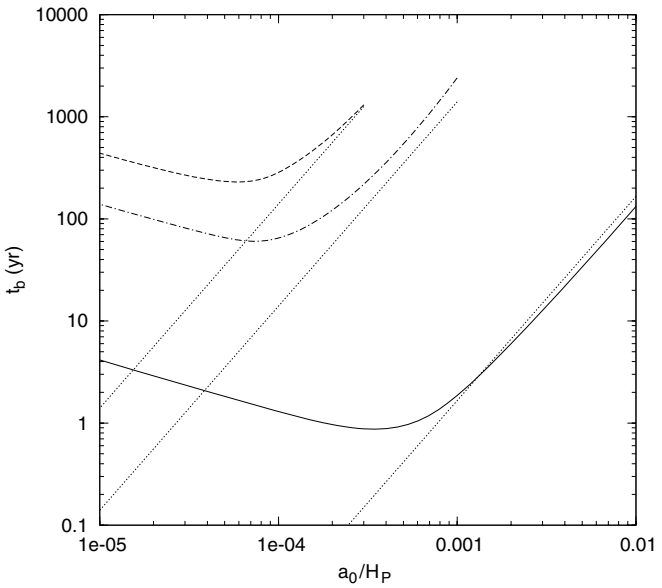

Figure 3. Dashed and dot-dashed curves show the dependences of the buoyant rising time on the ring cross-section radius for the rings with $\beta_0 = 10^8$ and $\beta_0 = 10^7$, respectively, whose chemical composition has not been changed by nuclear reactions ($\Delta\mu = \mu_e - \mu = 0$), while the solid curve corresponds to the ring with $\beta_0 = 10^{10}$ and $\Delta\mu = 5 \times 10^{-5}$ (μ reduced by ^{3}He burning). These three curves represent our numerical solutions of Equations (9)–(11). The dotted lines give their corresponding approximations by Equation (15), in which β_0 has been replaced by $\beta_{\rm eff} = \delta\mu^{-1} = (\mu/\Delta\mu)$ for the third case.

now controlled by the μ difference alone. Let us neglect, for a moment, the difference in temperature between the surrounding medium and the ring, $\delta T \equiv (T_e - T)/T_e \approx 0$. The buoyant acceleration is $a_b \approx g\delta\rho$. In the case of $\Delta\mu = 0$, the initial positive difference in density $\delta\rho \approx \delta P \approx \beta_0^{-1}$ is simply due to the excess magnetic pressure inside the ring (Equation (12)). On the other hand, in the case of $\Delta\mu > 0$, and for a weak toroidal field ($\delta P \approx 0$), we have $\delta\rho \approx \delta\mu \equiv \Delta\mu/\mu_e$. We can introduce the effective toroidal magnetic field $B_{\rm eff}$ associated with a specified value of $\delta\mu$ such that $\delta\mu = \beta_{\rm eff}^{-1}$. It turns out that $B_{\rm eff} \approx 9.8$ MG for $\Delta\mu = 5 \times 10^{-5}$ at $r = r_{\rm mix}$ in our RGB model. Hence, toroidal magnetic fields with $(B_\varphi)_0 \ll B_{\rm eff}$ will have a negligible effect on the motion of the ring with the reduced μ. For $\Delta\mu = 5 \times 10^{-5}$, $\beta_0 = 10^{10}$, and $a_0 = 10^{-3}$ the rising time $t_b \approx 1.6$ yrs is still short. However, it increases up to $t_b \approx 33$ yrs and $t_b \approx 132$ yrs for rings with the initial radii $a_0 = 5 \times 10^{-3}$ and $a_0 = 10^{-2}$, respectively, following the dependence $t_b \propto a_0^2$ for the thicker rings (Equation (15)).

The role that the reduced μ plays in the acceleration of the buoyant rise of the ring containing a weak magnetic field can be elucidated if we consider, for simplicity, that the ring's vertical motion consists of the following recurring sequence. Initially, let the ring have $\delta T = 0$ but $\delta\mu > 0$, hence $\delta\rho = \delta\mu + \beta_0^{-1} > 0$. Now, let the ring rise adiabatically until the accumulated difference in T compensates that in ρ, i.e., $\delta T = \delta\rho$. At this moment, the ring stops and waits a while for the heat exchange to make $\delta T = 0$ before starting to rise adiabatically again, and so on. But the waiting time is in fact the thermal time $\tau_{\rm th}$; therefore, it is inversely proportional to the heating rate dS/dt that linearly depends on the ratio $\delta T/a^2$ (Equation (14)). When the ring stops, it has $\delta T = \delta\mu + \beta_0^{-1}$. Therefore, if $\delta\mu \gg \beta_0^{-1}$ then $\delta T \approx \delta\mu$; hence we have $t_b \propto \tau_{\rm th} \propto \delta\mu^{-1} a^2 = \beta_{\rm eff} a^2$. On the other hand, if $\delta\mu \ll \beta_0^{-1}$ then $\delta T \approx \beta_0^{-1}$, and $t_b \propto \tau_{\rm th} \propto \beta_0 a^2$ (Equation (15)). The transition from the one to the other regime occurs at $\beta_0^{-1} \approx \delta\mu = \beta_{\rm eff}^{-1}$.

We have checked that Equation (15) gives a correct order-of-magnitude estimate (this time, at $a_0 \gtrsim 8 \times 10^{-4}$ though) for the buoyant rising time of a ring with a reduced μ provided that β_0 is replaced by $\beta_{\rm eff} = \delta\mu^{-1}$ (the dotted line approximating the solid curve in Figure 3). It is also important to note that the coefficients in Equations (15)–(16) have been obtained for a particular RGB model (our model from Table 1); therefore, they are model dependent. For example, given that t_b is expected to be inversely proportional to the thermal diffusivity K as well (Equation (14)), the latter being roughly proportional to the luminosity, we predict that these coefficients should change by a factor of 10 (t_b decreases, while $\langle v_b \rangle$ increases) toward the RGB tip ($\log L/L_\odot \approx 3.3$). This scaling is indeed confirmed by our computations.

6.3. Comparison with Results Obtained by BWNC

Given that one rising magnetic flux ring carries the mass $m_b = 2\pi^2 r_0 a_0^2 \rho_0 \sin\theta_0 = 2\pi^2 r a^2 \rho \sin\theta$, N such rings present in the radiative zone at the same time will provide chemical mixing with the mass rate

$$\dot{M}_b = \frac{N m_b}{t_b}, \tag{17}$$

where t_b is their buoyant rising time. The quantity $\dot{M}_b$ has to match the observationally constrained rate of the RGB extra mixing $\dot{M}_{\rm mix} \approx 4 \times 10^{-8}\ M_\odot\ {\rm yr}^{-1}$ (BWNC). The right-hand side of Equation (17) is a function of the ring parameters N, a_0, and $(B_\varphi)_0$. For a ring with a reduced μ, the third parameter should be replaced with $\Delta\mu$, unless $\delta\mu \ll 1/\beta_0$ (Section 6.2). In the case of $\Delta\mu = 0$, considered by BWNC, the equating of $\dot{M}_b$ to $\dot{M}_{\rm mix}$ gives a relationship between N, a_0, and $(B_\varphi)_0$. To estimate a reasonable value of a_0 at $r = r_{\rm mix}$, they have referred to the characteristic dimension $a_\odot \sim$ 1000–2000 km of magnetic flux tubes that are believed to exist deep in the solar convective zone. Besides the RGB model, they have also considered a representative model for low-mass asymptotic giant branch (AGB) stars, whose structure above the H burning shell resembles that of upper RGB stars. There is indirect evidence, such as distinctive ^{18}O/^{16}O, ^{17}O/^{16}O, ^{12}C/^{13}C, and N/C abundance ratios in the meteorite grains of AGB circumstellar origin (Wasserburg et al. 2006) and in the atmospheres of carbon-enhanced metal-poor stars (Ryan et al. 2005; Sivarani et al. 2006; Masseron et al. 2006; Denissenkov & Pinsonneault 2008a; Lebzelter et al. 2008), indicating that extra mixing may also operate in the radiative zones of these stars (Nollett et al. 2003). In their RGB-1 and RGB-2 magnetic buoyancy models, BWNC have employed the values of a_0 obtained assuming that $a(r_{\rm bce}) = a_\odot$ and using Equation (13) with the stellar structure parameters from their AGB and RGB stellar models, respectively. These values are listed in our Table 2 along with the corresponding estimates for our RGB model.

BWNC have also assumed that there is only one magnetic flux ring floating in the radiative zone at any time. Substituting the number $N = 1$ together with the values of a_0 from Table 2 and $\dot{M}_{\rm mix} = 4 \times 10^{-8}\ M_\odot\ {\rm yr}^{-1}$ into Equation (17) constrains the required values for t_b and $\langle v_b \rangle$ (Table 2). Under the assumptions, made by BWNC, that the ring always stays in the thermal equilibrium with its surrounding medium ($\delta T = 0$) and that the only force impeding its motion is the aerodynamic drag force, it is easy to show that $t_b \propto \sqrt{\beta_0/a_0} \propto (B_\varphi)_0/\sqrt{a_0}$.

It is from the last relation that BWNC have determined the toroidal field strengths needed to drive the RGB extra mixing by magnetic buoyancy (Table 2, $(B_\varphi)_0$ is transformed to $(B_\varphi)_{\rm bce}$ using Equation (13)). They pointed out that these results are consistent with existing observations of magnetic fields in red giants (e.g., Blackman et al. 2001).

However, as we have noted, BWNC underestimated the ring's rising time by assuming that the heat exchange between the surrounding medium and the ring occurs instantaneously, which maintains $\Delta T = 0$ all the time. Our more conservative assumption explicitly takes into consideration the radiative heat exchange, which leads to a much longer ring's rising time, as approximated by Equation (15). Employing the values of a_0, $t_{\rm b}$, and β_0 from columns RGB-1 and RGB-2 of Table 2, we find that the rising times have been underestimated by the factors 6×10^4 and 4×10^6 for these buoyancy models. To keep the same estimates for the toroidal field strength, the ring number N has to be increased by the corresponding factors. However, the volume occupied by $\sim 10^5$–10^6 rings is comparable to the total volume of the radiative zone, in which case the stellar structure would be greatly disturbed, especially at the bottom of convective envelope where the rings encounter turbulent convection. Here, the frozen-in toroidal field is either quickly dissipated via the strong turbulent diffusion, thus depositing its energy at the radiative/convective interface, or it inhibits convective motions if its potential energy exceeds the turbulent kinetic energy (Moss 2003). In either case, the stellar structure would be strongly modified. In the next section, we will show that a reasonably small number of N can be obtained only for rings with a reduced μ.

6.4. There Still May Be a Solution

By assigning $N = 1$, BWNC have implicitly assumed that the average time $t_{\rm form}$ needed to form a magnetic flux ring is equal to its buoyant rising time $t_{\rm b}$. Indeed, instead of (17) the buoyancy mixing mass rate ought to be calculated as $\dot{M}_{\rm b} = m_{\rm b}/t_{\rm form} = N m_{\rm b}/t_{\rm b}$, where $N = t_{\rm b}/t_{\rm form}$. We assume that, like in the case of the solar tachocline (e.g., Schmitt & Rosner 1983), the appropriate MHD mechanism responsible for the formation of magnetic flux rings in the vicinity of the H burning shell is the undular buoyancy instability. The criterion for its development has been extensively discussed in the literature, e.g., by Acheson (1978), Spruit & van Ballegooijen (1982), Spruit (1999), and Fan (2001). It has been shown that a diffusive toroidal magnetic field gets broken into distinct arching flux tubes when

$$B_\varphi > (B_\varphi)_{\rm crit} \approx \sqrt{4\pi\rho\, r^2 N^2\, \frac{H_P}{r}\, \frac{\eta}{K}}, \qquad (18)$$

provided that $(\partial \ln B_\varphi/\partial \ln r) = O(1)$. A profile of $(B_\varphi)_{\rm crit}$ in the radiative zone of our RGB model is plotted with the dashed curve in Figure 4(a). Its corresponding profile of $\beta_{\rm crit}$ is shown with the dot-dashed curve. At $r = r_{\rm mix}$ ($\log r_{\rm mix}/R_\odot \approx -1.30$), the critical toroidal field is 254 kG and $\beta_{\rm crit} = 1.8 \times 10^7$ (Table 2).

In the presence of rapid rotation, such that $\Omega \gg \omega_{{\rm A},\varphi} \equiv B_\varphi/(\sqrt{4\pi\rho}\, r)$, the Coriolis force reduces the instability's growth rate $\omega_{{\rm A},\varphi}$ by the factor $\omega_{{\rm A},\varphi}/\Omega$ (Pitts & Tayler 1985; Spruit 1999). In our RGB model, $\Omega(r_{\rm mix}) = 10^{-3}$ rad s^{-1} strongly exceeds $\omega_{{\rm A},\varphi}\,(r_{\rm mix}) = 2.11 \times 10^{-11}\, B_\varphi$ rad s^{-1} for all reasonable strengths of $B_\varphi \ll 47$ MG. Therefore, we use the estimate of $t_{\rm inst} \approx \Omega/\omega^2_{{\rm A},\varphi}$ for the instability growth time. The winding up of a toroidal field by differential rotation continues until $B_\varphi \approx \Omega B_r \Delta t\, q$ reaches the critical value (18). This takes $(\Delta t)_{\rm crit} \approx 3.17 \times 10^{-3}\, (B_\varphi)_{\rm crit}/(B_r\, \Omega_{-5}\, q)$ years. After that, it will take another $t_{\rm inst} \approx 1.93 \times 10^{10} \left[\rho\, (r/R_\odot)^2\, \Omega_{-5}\right]/(B_\varphi)^2_{\rm crit}$ years for the buoyancy instability to occur and assemble the rings. So, the total ring-formation time is $t_{\rm form} = (\Delta t)_{\rm crit} + t_{\rm inst}$. For our simple estimates to be true, $t_{\rm form}$ should be shorter than $\omega^{-1}_{{\rm A},r} = 7.82 \times 10^3\, \sqrt{\rho}\, (r/R_\odot)/B_r$ yrs, which allows us to consider that the rotational shear is nearly constant and that, for our assumed rotation law in the radiative zone $\Omega_{-5} = 10^2\, (r_{\rm mix}/r)^2$, $q = O(1)$. For this case, and assuming that $B_r = 7.32\, (r_{\rm mix}/r)^2$ G, the four characteristic timescales are plotted in Figure 4(b). In particular, we have $t_{\rm form} = 2.20$ yrs at $r = r_{\rm mix}$. Note that $(\Delta t)_{\rm crit} \propto (B_r \Omega)^{-1}$, $t_{\rm inst} \propto \Omega$, and $\omega^{-1}_{{\rm A},r} \propto B_r^{-1}$. We have used the parameter $B_r(r_{\rm mix}) = 7.32$ G for which the timescales $(\Delta t)_{\rm crit}$ and $t_{\rm inst}$ coincide. Its value scales as $\Omega^{-2}(r_{\rm mix})$. At a fixed value of $\Omega(r_{\rm mix})$, $B_r(r_{\rm mix})$ determines which of the two timescales, $(\Delta t)_{\rm crit}$ or $t_{\rm inst}$, makes a predominant contribution to $t_{\rm form}$.

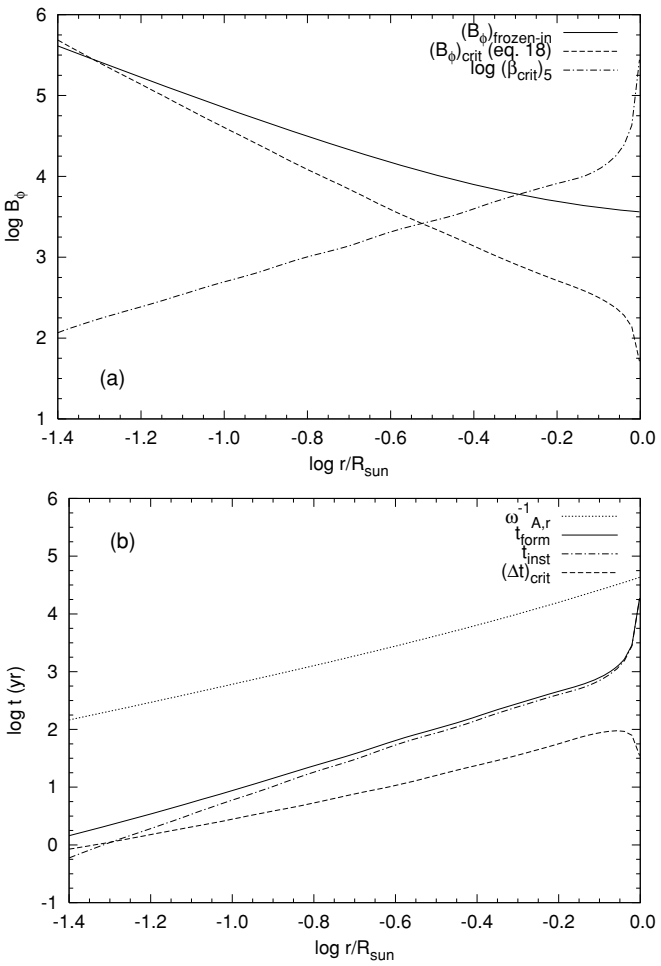

Figure 4. (a) Critical toroidal field (the dashed curve) and parameter β (the dot-dashed curve) for the triggering of the buoyancy instability (Equation (18)) and the evolution of the toroidal field strength in the rising ring (the solid curve, Equation (13)). (b) The timescales for the winding up of the critical toroidal field ($\Delta t_{\rm crit}$) and for the development of the buoyancy instability ($t_{\rm inst}$), as well as the total ring-formation time ($t_{\rm form} = \Delta t_{\rm crit} + t_{\rm inst}$). These timescales should be shorter than the toroidal field growth time $\omega^{-1}_{{\rm A},r}$. In these computations, it has been assumed that $B_r = 7.32\, (r_{\rm mix}/r)^2$ G, which makes $(\Delta t)_{\rm crit} = t_{\rm inst}$ at $r = r_{\rm mix}$, where $\log(r_{\rm mix}/R_\odot) \approx -1.30$.

It is very likely that the buoyancy instability forms not just one but a number $n > 1$ of magnetic flux rings during the time $t_{\rm form}$, therefore $N = n(t_{\rm b}/t_{\rm form})$. The equating of $\dot{M}_{\rm b} = nm_{\rm b}/t_{\rm form}$ to $\dot{M}_{\rm mix} = 4 \times 10^{-8}\ M_\odot\ {\rm yr}^{-1}$ constrains the ring's minimum radius as a function of $t_{\rm form}$, n, and the initial colatitude

$$\left(\frac{a_0}{H_P}\right)^2 = \frac{\dot{M}_{\rm mix}\, t_{\rm form}}{n\, 2\pi^2 r_0^3 \rho_0 \sin\theta_0}\left(\frac{H_P}{r_0}\right)^{-2} = 9.78 \times 10^{-5}\frac{t_{\rm form}}{n\ \sin\theta_0}, \quad (19)$$

where $r_0 = r_{\rm mix}$, and $t_{\rm form}$ is expressed in years.

For the values of $t_{\rm form} = 2.20$ yrs, $n = 1$, and $\theta_0 = 90^\circ$, we calculate $a_0 = 1.47 \times 10^{-2}$ (in units of H_P, as usual), and the total number of rings in the radiative zone $N = 0.454\, t_{\rm b}$. As mentioned before, the ring with the radius $a_0 = 10^{-2}$ and μ reduced by $\Delta\mu = 5 \times 10^{-5}$ has the buoyant rising time $t_{\rm b} \approx 132$ yrs. This means that the ring with $a_0 = 1.47 \times 10^{-2}$ and the same mean molecular weight would cross the radiative zone in $t_{\rm b} \approx (1.47)^2 \times 132 = 285$ yrs (Equation (15)). Hence, we have $N = 129$. Note that this number does not change if the values of the parameters $t_{\rm form}$ and n are varied, provided that our buoyancy mixing mass rate is still constrained to match $\dot{M}_{\rm mix}$. Indeed, in this case both the ratios $t_{\rm form}/n$ (Equation (19)) and $t_{\rm b}$ (Equation (15)) are proportional to a_0^2, which leads to its cancellation in the relationship $N = n(t_{\rm b}/t_{\rm form})$.

We have shown that the reduced mean molecular weight in the magnetic flux rings formed in the region of ^{3}He burning accelerates their buoyant rise quickly enough for their total number needed to maintain the RGB extra mixing to be reasonably small ($N \approx 10^2$ rings would only occupy $\sim 10^{-3}$–10^{-4} part of the radiative zone). However, the estimated value of $N \approx 1.3 \times 10^2$ is in fact a lower limit obtained under the most favorable assumptions. In particular, we have silently assumed that all rings have the same formation time and cross-section radius related by Equation (19), and that no rings are formed above the radius $r_{\rm mix}$. These assumptions are obviously not true. Relaxing either of them will certainly increase the total ring number in the radiative zone. To figure out what effect may be produced by relaxing the first assumption, we would have to determine a relationship between $t_{\rm form}$ and a_0 for a spectrum of rings created by the buoyancy instability, e.g., like it has been done for the solar tachocline by Schmitt & Rosner (1983). This problem is out of scope of the present preliminary study.

We find it more important to address here the second issue. Indeed, given that the critical strength of toroidal magnetic field for triggering the buoyancy instability decreases rapidly with the radius (the dashed curve in Figure 4(a)), while our estimated ring-formation time stays much shorter than the toroidal field growth time $\omega_{{\rm A},r}^{-1}$ (Figure 4(b)), the formation of magnetic flux rings at $r_0 > r_{\rm mix}$ appears to be unavoidable. These rings would contribute to the total ring number present in the radiative zone at the same time but they would not participate in the chemical element transport because their constituent material has not been nuclearly processed. In fact, the buoyancy of these "parasitic" rings should be reduced compared to the buoyancy of the rings originating at $r \approx r_{\rm mix}$ because their mean molecular weight does not differ from that of the surrounding medium through which they rise. On the other hand, they are formed in a region where the thermal diffusivity K is higher than at $r = r_{\rm mix}$ and, therefore, their heat exchange with the surroundings goes faster, which should accelerate their buoyant rise. Our computations show that the rings formed in the region of constant μ (at $r \gtrsim r_{\rm mix} + 0.05\ R_\odot$) rise 10^3 to 10^4 times slower than the rings formed in the μ-depression domain. Given that their formation takes between 10 and 100 yrs (the solid curve in Figure 4(b)), a number of the "parasitic" rings present in the radiative zone at the same time may be as large as 10^5. Unfortunately, our model is too simple to be able to predict if and how the "parasitic" rings could impede the large-scale magnetic buoyancy mixing, but we do realize that they may create a real problem for the mechanism proposed by BWNC that has been revised in our paper. Indeed, although BWNC did not discuss a formation of magnetic rings, it is difficult to understand why the rings cannot be formed at $r > r_{\rm mix}$ as easily as they are created at $r = r_{\rm mix}$.

7. DISCUSSION

Our approximate analysis of the magnetic flux ring formation and buoyant rise in the differentially rotating radiative zone of the bump luminosity RGB star gives some support to a combined "magneto-thermohaline" mode of the RGB extra mixing, as opposed to the pure thermohaline and pure magnetic buoyancy modes proposed by Charbonnel & Zahn (2007a) and BWNC, respectively. A key component to the operation of our mixing mechanism, which is certainly present in all upper RGB and low-mass AGB stars, is the mass inflow in the radiative zone. It makes two important things. First, the conservation of the specific angular momentum in the mass inflow results in a steep Ω-profile with a rotational shear $q \approx O(1)$ that does not appear to be strongly reduced by the meridional circulation and turbulent diffusion (Denissenkov & Tout 2000; Palacios et al. 2006). Second, the mass inflow entrains a diffusive magnetic field that is probably generated via an α–Ω or α^2 dynamo just beneath the bottom of convective envelope (Nordhaus et al. 2007; Nordhaus & Blackman 2007; Mestel 2001). A very high ratio of the ohmic dissipation time to the average inflow time $((\Delta r)^2/\langle\eta\rangle)/(\Delta r/\langle|\dot{r}|\rangle) \approx 1.2 \times 10^4$ guarantees that this field will be redistributed over the whole radiative zone. Because the volume occupied by this field is squeezed when the flow approaches the H burning shell, the field may become stronger at a smaller radius. In general, this random field has an unstable configuration that will decay on a short Alfvén timescale (Spruit 1999). However, in their 3D MHD simulations Braithwaite & Nordlund (2006) have shown that such unstable random field may evolve into a stable "twisted torus" configuration with toroidal and poloidal field components of comparable strength. The poloidal field lines get wrapped around an axisymmetric torus, thus forming an approximate dipole. These simulations have provided the first plausible explanation of the origin and stability of dipole magnetic fields in presently nonconvective stars. It is assumed that the seed random magnetic field in those stars had been a dynamo left over from the period of their protostellar convective contraction.

Our RGB extra mixing model has much in common with the solar magnetic spindown model that postulates the presence of a weak poloidal field in the solar radiative core (Mestel & Weiss 1987; Charbonneau & MacGregor 1993). Note that even the values of $r_{\rm bce} = 0.996\, R_\odot$ and $\Omega(r_{\rm bce}) = 10^{-6}$ rad s^{-1} used in our RGB model are close to the corresponding solar values. The important difference is the assumption of strong differential rotation in the radiative zone of our model, while the present-day Sun is known to be a nearly solid-body rotator, at least above $r = 0.2\ R_\odot$ (Couvidat et al. 2003). However, the young Sun did possess a strong differential rotation in the core which had resulted from its spinning up during the pre-MS contraction

and angular momentum loss from the surface via a magnetized stellar wind. The magnetic spindown model assumes that the differential rotation in the young Sun was broken by the back reaction of the Lorentz force that emerged when the differential rotation was winding up a toroidal field from the preexisting poloidal field (Charbonneau & MacGregor 1993), or by the magneto-rotational instability (Menou & Le Mer 2006).

Whereas an important role in damping large-scale toroidal field oscillations in the young Sun is thought to be played by the phase mixing (Charbonneau & MacGregor 1993), we do not think that this is also true for our magnetic buoyancy model. Indeed, the phase mixing timescale at $r = r_{\rm mix}$ in our RGB stellar model is

$$t_{\rm p} = \left(\frac{3\pi^3 r^2}{\eta\omega_{{\rm A},r}^2 q_{\rm A}^2}\right)^{1/3} \approx 2.9\times10^5 \ \ {\rm yrs}, \qquad (20)$$

where we have used an estimate of $t_{\rm p}$ obtained by Spruit (1999), assuming that $q_{\rm A} = 1$. This is comparable with the time needed for the whole radiative zone to be thoroughly mixed, $t_{\rm mix} = (M_{\rm bce} - M_{\rm mix})/\dot{M}_{\rm mix} \approx 5.5\times10^5$ yrs. Hence, long before the toroidal field oscillations on neighboring magnetic surfaces get out of phase, the magnetic buoyancy instability will come into play, the magnetic flux rings will be formed and reach the convective envelope.

Compared with the pure thermohaline mixing, our model has the following advantages. First, the horizontal turbulent diffusion is unlikely to hinder the buoyant rise of magnetic flux rings with a reduced μ because the frozen-in toroidal field will not allow turbulence to penetrate plasma in the rings and decrease the μ contrast between the ring and surrounding material. On the contrary, there is nothing to prevent the horizontal turbulent diffusion from eroding the μ contrast in thermohaline convective elements (Section 4).

Second, thermohaline convection may fail to explain the operation of enhanced extra mixing in rapidly rotating Li-rich K-giants, which is needed to activate the Cameron–Fowler mechanism, because one would expect that the growth of "salt fingers" is impeded by rotation (Canuto 1999). Oppositely, it would be natural to suppose that magnetic flux rings are formed more efficiently in the more rapidly rotating stars. This hypothesis is supported by the fact that the fastest rotators among young cluster solar-type stars appear to have the shortest timescale of rotational coupling between the core and envelope (e.g., Irwin et al. 2007).

Third, whereas the efficiency of thermohaline convection in upper RGB stars is dependent exclusively on the abundance of ^{3}He left in the radiative zone, magnetic buoyancy can, in principle, be driven by differential rotation alone, provided that it succeeds in winding up a sufficiently strong toroidal field. By the end of the RGB evolution of a low-mass star, its envelope ^{3}He abundance gets depleted by a factor of ten or more (Charbonnel & Zahn 2007a). So, what will then drive extra mixing in this star on the AGB? The higher rate of heat exchange between "salt fingers" and their surrounding medium increased in proportion to the luminosity will not help because the evolutionary timescale decreases inversely proportional to the luminosity which cancels the former effect. Thus, there is a need for an additional driving parameter that would not let extra mixing die out. Such parameter might be the rotational velocity. Indeed, it is known that a surprisingly fast rotation has somehow survived in red horizontal branch stars in spite of the RGB mass loss (Peterson 1983; Sills & Pinsonneault 2000; Behr et al. 2003). It could be used on the subsequent AGB evolutionary phase to drive our magneto-thermohaline mixing. The much lower (compared to the RGB phase) ^{3}He abundance left in these stars could be compensated by a stronger toroidal magnetic field or a larger number of magnetic flux rings generated in the presence of a higher mass inflow rate ($\dot{M}_{\rm mix} \approx 10^{-6}\ M_\odot\ {\rm yr}^{-1}$, according to BWNC).

Fourth, thermohaline convection cannot penetrate below the radius $r_{\rm min} \approx 0.063\ R_\odot$ at which μ has a minimum (the right vertical dotted line in Figure 1). However, mixing down to this depth would be too shallow to reduce the surface carbon abundance (Figure 1(a)), as required by observations (Gratton et al. 2000; Smith & Martell 2003). An overshooting on a length scale of order H_P could solve the problem (the left vertical dotted line in Figure 1 is placed at a distance H_P below $r_{\rm min}$) but then thermohaline "fingers" would have to penetrate a region of higher μ where they experience a strong breaking. It should also be noted that the penetration of a region with the positive ∇_μ below $r_{\rm min}$ would reduce the average mixing rate $D_{\rm thc} \propto |\nabla_\mu|$ by decreasing the slope of the negative ∇_μ in the mixed radiative zone. In the magnetic buoyancy model, there is at least a potential possibility to dredge up the nuclearly processed material from below $r_{\rm min}$. This can be done by rings with a frozen-in magnetic field of a few MG if such are formed closer to the major H burning shell. Of course, all the above assumptions need to be verified by more rigorous models.

Fifth, it is interesting to note that the operation of our RGB mixing mechanism seems to produce environment in which the functioning of the ^{3}He-driven thermohaline convection is impossible. Indeed, Charbonnel & Zahn (2007b) have estimated that a toroidal magnetic field of $B_\varphi \approx 100$ kG would entirely suppress the thermohaline mixing at $r \approx r_{\rm mix}$, while a field of 10 kG would be sufficient to inhibit the thermohaline instability in the upper one-third of the narrow μ-depression domain. These fields are weaker than those needed for our mechanism to work.

It is also important to note that the flux rings considered in our paper are a convenient proxy for the more realistic Ω-shaped loops that are the likely products of the magnetic buoyancy instability that operates in a layer of strong toroidal field (e.g., Caligari et al. 1995). Downflows/upflows that take place in the loop legs during formation and rise may affect the efficiency of transport of processed material relative to the behavior obtained in the case of a flux ring. It is not clear how the strong rotational shear that is present within the radiative zone would affect this process. In principle, the only place where significant shear is required is within the layers where μ is depressed and flux tube formation takes place. If the overlying portion of the radiative zone were in a state of near-uniform rotation, the loop legs might form a kind of conduit connecting the region containing processed material with the bottom of the convection zone. In any case, it is difficult to give an airtight argument for what the rotational state of the radiative zone should be, either differential rotation of the kind assumed in our paper or near-uniform rotation enforced by the fields that permeate the region.

Another aspect of our computations that should be noted is that the results of Sections 6.1 and 6.2 were obtained for rings initially in thermal equilibrium with their surroundings, a state of maximal initial buoyancy. If, alternatively, the rings were in an initial mechanical equilibrium state (zero net force), the rise would be slower by virtue of the heating required to overcome the neutral buoyancy at $t = 0$. This would also increase the total ring number.

8. CONCLUSION

In this work, we have presented a simple model of the formation and buoyant rise of magnetic flux rings in the radiative zone of the bump luminosity RGB star. Our model is based on ideas and equations published by Spruit & van Ballegooijen (1982), Schmitt & Rosner (1983), Mestel & Weiss (1987), Choudhuri & Gilman (1987), Charbonneau & MacGregor (1993), Spruit (1999), Eggleton et al. (2006), BWNC, and Denissenkov & Pinsonneault (2008b). It qualitatively describes a possible mechanism for the RGB extra mixing, which we call the magneto-thermohaline mixing, as an alternative to the pure ^{3}He-driven thermohaline convection that has recently been proposed by Charbonnel & Zahn (2007a). For our mechanism to work, the radiative zone has to possess a strong differential rotation and a poloidal magnetic field $B_{\rm p} \gtrsim 1$–10 G. We assume that the differential rotation stretches the poloidal field around the rotation axis, thus creating a strong toroidal magnetic field $B_\varphi \approx 0.1$–1 MG. When the latter exceeds a critical value, the buoyancy-related undular instability comes into play to form magnetic flux rings. These rings turn out to be buoyant, therefore they rise toward the bottom of convective envelope.

We have shown that, when the radiative heat exchange between the ring and its surrounding medium is taken into account, the ring's buoyant rising time increases by about five orders of magnitude compared to the case considered by BWNC, when the ring and its surrounding medium are assumed to be in thermal equilibrium all the time. However, given that our model still neglects possible internal heating of the ring's material by residual nuclear reactions and anisotropic thermal exchanges in the presence of strong oriented magnetic field, while it uses the aerodynamic drag coefficient that is 20 times as large as the one employed by BWNC, it is fair to say that BWNC might have fixed a safe upper limit while our paper fixes a conservative lower limit for the magnetic ring's rising velocity.

We have found that the number of rings needed to be present in the radiative zone at the same time to produce the observationally constrained rate of the RGB extra mixing is unrealistically large unless these rings originate from the region of the μ inversion maintained by the ^{3}He burning. Such rings have a deficit of the mean molecular weight compared to the bulk of the radiative zone through which they move. Their buoyancy is mainly caused by the difference in μ rather than by a deficit in density due to the excess magnetic pressure. The frozen-in toroidal magnetic field is still needed for the rings to remain cohesive while rising. That is why we have coined the term "magneto-thermohaline" mixing. Our model has some advantages over the pure thermohaline mixing model, the most important of which being the robustness of the magnetic rings against the eroding effect produced by the horizontal turbulent diffusion. Leaving aside the problem of the "parasitic" rings that are formed at $r \gtrsim r_{\rm mix} + 0.05\,R_\odot$, our model looks promising. However, because it is based on a number of assumptions whose legality is impossible to confirm in the framework of our 1D computations we call for its future verification by 3D MHD simulations.

P.A.D. and M.P. acknowledge support from the NASA grant NNG05 GG20G. The National Center for Atmospheric Research is sponsored by the National Science Foundation.

REFERENCES

Acheson, D. J. 1978, Phil. Trans. R. Soc. Lond. A, 289, 459
Aoki, W., et al. 2008, ApJ, 678, 1351
Behr, B. B. 2003, ApJS, 149, 101
Blackman, E. G., Frank, A., Markiel, J. A., Thomas, J. H., & Van Horn, H. M. 2001, Nature, 409, 485
Braithwaite, J., & Nordlund, Å. 2006, A&A, 450, 1077
Busso, M., Wasserburg, G. J., Nollett, K. M., & Calandra, A. 2007, ApJ, 671, 802 (BWNC)
Caligari, P., Moreno-Insertis, F., & Schussler, M. 1995, ApJ, 441, 886
Cameron, A. G. W., & Fowler, W. A. 1971, ApJ, 164, 111
Canuto, V. M. 1999, ApJ, 524, 311
Chaboyer, B., & Zahn, J.-P. 1992, A&A, 253, 173
Chanamé, J., Pinsonneault, M., & Terndrup, D. M. 2005, ApJ, 631, 540
Charbonneau, P., & MacGregor, K. B. 1993, ApJ, 417, 762
Charbonnel, C., & Balachandran, S. C. 2000, A&A, 359, 563
Charbonnel, C., Brown, J. A., & Wallerstein, G. 1998, A&A, 332, 204
Charbonnel, C., & Do Nascimento, J. D., Jr. 1998, A&A, 336, 915
Charbonnel, C., & Zahn, J.-P. 2007a, A&A, 467, L15
Charbonnel, C., & Zahn, J.-P. 2007b, A&A, 476, L29
Choudhuri, A. R., & Gilman, P. A. 1987, ApJ, 316, 788
Couvidat, S., García, R. A., Turck-Chièze, Corbard, T., Henney, C. J., & Jiménez-Reyes, S. 2003, ApJ, 597, L77
Denissenkov, P. A., & Tout, C. A. 2000, MNRAS, 316, 395
Denissenkov, P. A., & VandenBerg, D. A. 2003, ApJ, 593, 509
Denissenkov, P. A., & Herwig, F. 2004, ApJ, 612, 1081
Denissenkov, P. A., Chaboyer, B., & Li, K. 2006, ApJ, 641, 1087
Denissenkov, P. A., & Pinsonneault, M. 2008a, ApJ, 679, 1541
Denissenkov, P. A., & Pinsonneault, M. 2008b, ApJ, 684, 626
Denissenkov, P. A., & Weiss, A. 1996, A&A, 308, 773
Drake, N. A., de la Reza, R., da Silva, L., & Lambert, D. L. 2002, AJ, 123, 2703
Eggleton, P. P., Dearborn, D. S. P., & Lattanzio, J. C. 2006, Science, 314, 1580
Fan, Y. 2001, ApJ, 546, 509
Gratton, R. G., Sneden, C., Carretta, E., & Bragaglia, A. 2000, A&A, 354, 169
Irwin, J., Hodgkin, S., Aigrain, S., Hebb, L., Bouvier, J., Clarke, C., Moraux, E., & Bramich, D. M. 2007, MNRAS, 377, 741
Kippenhahn, R., Ruschenplatt, G., & Thomas, H.-C. 1980, A&A, 91, 175
Lebzelter, T., Lederer, M. T., Cristallo, S., Hinkle, K. H., Straniero, O., & Aringer, B. 2008, A&A, 486, 511L
MacDonald, J., & Mullan, D. J. 2004, MNRAS, 348, 702
MacGregor, K. B., & Cassinelli, J. P. 2003, ApJ, 586, 480
Maeder, A. 2003, A&A, 399, 263
Masseron, T. 2006, A&A, 455, 1059
Menou, K., & Le Mer, J. 2006, ApJ, 650, 1208
Mestel, L. 2001, in ASP Conf. Ser. 248, Magnetic Fields across the Hertzsprung-Russel Diagram, ed. G. Mathys, S. K. Solanki, & D. T. Wickramasinghe (San Francisco, CA: ASP), 3
Mestel, L., & Weiss, N. O. 1987, MNRAS, 226, 123
Moss, D. 2003, A&A, 403, 693
Newsham, G., & Terndrup, D. M. 2007, ApJ, 664, 332
Nollett, K.-M., Busso, M., & Wasserburg, G. J. 2003, ApJ, 582, 1036
Nordhaus, J., & Blackman, E. G. 2008, in AIP Conf. Proc. 1001, IXth Torino Workshop on Evolution and Nucleosynthesis in AGB Stars and the IInd Perugia Workshop on Nuclear Astrophysics (New York: AIP), 306
Nordhaus, J., Blackman, E. G., & Frank, A. 2007, MNRAS, 376, 599
Palacios, A., & Brun, A. S. 2006, in IAU Symp. 239, Convection in Astrophysics, ed. F. Kupka, I. Roxburgh, & K. L. Chan (Dordrecht: Kluwer), 431 (arXiv:astro-ph/0610040v1)
Palacios, A., Charbonnel, C., Talon, S., & Forestini, M. 2003, A&A, 399, 603
Palacios, A., Charbonnel, C., Talon, S., & Siess, L. 2006, A&A, 453, 261
Peterson, R. C. 1983, ApJ, 275, 737
Pitts, E., & Tayler, R. J. 1985, MNRAS, 216, 139
Ryan, S. G., Aoki, W., Norris, J. E., & Beers, T. C. 2005, ApJ, 635, 349
Schmitt, J. H. M. M., & Rosner, R. 1983, ApJ, 265, 901
Siess, L., Dufour, E., & Forestini, M. 2000, A&A, 358, 593
Sills, A., & Pinsonneault, M. H. 2000, ApJ, 540, 489
Sivarani, T., et al. 2006, A&A, 459, 125
Smith, G. H., & Martell, S. L. 2003, PASP, 115, 1211
Spruit, H. C. 1999, A&A, 349, 189
Spruit, H. C., & van Ballegooijen, A. A. 1982, A&A, 106, 58
Stern, M. E. 1960, Tellus, 12, 172
Sweigart, A. V., & Mengel, J. G. 1979, ApJ, 229, 624
Talon, S., & Zahn, J.-P. 1997, A&A, 317, 749
Talon, S., Zahn, J.-P., Maeder, A., & Meynet, G. 1997, A&A, 322, 209
Ulrich, R. K. 1972, ApJ, 172, 165
Vauclair, S. 2004, ApJ, 605, 874
Wasserburg, G. J., Busso, M., Gallino, R., & Nollett, K. M. 2006, Nucl. Phys. A, 777, 5
Zahn, J.-P. 1992, A&A, 256, 115